JACS Au
AN OPEN ACCESS JOURNAL OF THE AMERICAN CHEMICAL SOCIETY

pubs.acs.org/jacsau
Article

Connecting Protein Millisecond Conformational Dynamics to Protein Thermal Stability

Xue-Ni Hou, Bin Song, Chang Zhao, Wen-Ting Chu, Mei-Xia Ruan, Xu Dong, Ling-Shen Meng, Zhou Gong, Yu-Xiang Weng, Jie Zheng,* Jin Wang,* and Chun Tang*

Cite This: JACS Au 2024, 4, 3310−3320
Read Online
ACCESS | Metrics & More | Article Recommendations | Supporting Information

ABSTRACT: The stability of protein folded states is crucial for its function, yet the relationship with the protein sequence remains poorly understood. Prior studies have focused on the amino acid composition and thermodynamic couplings within a single folded conformation, overlooking the potential contribution of protein dynamics. Here, we address this gap by systematically analyzing the impact of alanine mutations in the C-terminal β-strand (β5) of ubiquitin, a model protein exhibiting millisecond timescale interconversion between two conformational states differing in the β5 position. Our findings unveil a negative correlation between millisecond dynamics and thermal stability, with alanine substitutions at seemingly flexible C-terminal residues significantly enhancing thermostability. Integrating spectroscopic and computational approaches, we demonstrate that the thermally unfolded state retains a substantial secondary structure but lacks β5 engagement, recapitulating the transition state for millisecond dynamics. Thus, alanine mutations that modulate the stabilities of the folded states with respect to the partially unfolded state impact both the dynamics and stability. Our findings underscore the importance of conformational dynamics with implications for protein engineering and design.

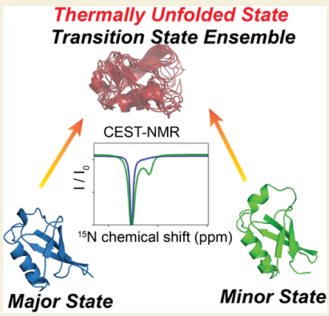

KEYWORDS: *thermostability, protein unfolding, conformational dynamics, ubiquitin, NMR, integrative spectroscopy*

INTRODUCTION

Under physiological conditions, structured proteins primarily exist in the folded state. The stability of protein folded state is crucial for its function, and the relationship between protein sequence and stability remains a fundamental question in biophysics, with implications in protein structure prediction and protein design.[1,2] At elevated temperatures, proteins can overcome energetic barriers and transition to unfolded states with the melting temperature (T_m) defining the point of 50% unfolding. However, protein unfolding is a complex multistep process, and bulk spectroscopic measurements during thermal denaturation may not fully resolve the contributing intermediate states. Moreover, these partially unfolded intermediates can impact protein aggregation propensity.[3,4] Thus, a comprehensive understanding of protein stability necessitates looking beyond amino acid fitness and thermodynamic coupling within a single folded conformation.

Protein conformational fluctuations span a vast range of time scales, from picoseconds to minutes, with microsecond to millisecond (μs−ms) dynamics being particularly relevant to protein function.[5−12] While protein folding often takes place on the μs−ms time scale, the rate of protein unfolding greatly varies depending on experimental conditions. Previous research has mostly focused protein unfolding under high concentrations of denaturant,[13−17] whereas the structural changes during thermal denaturation have been less explored.[18−20] Consequently, the extent of the structural transition during thermal unfolding and the relationship between protein dynamics in the native folded state and thermal stability are unclear.

Ubiquitin (Ub), a 76-residue small protein, serves as a model system in protein research and plays essential biological roles. Ub can form diverse polyubiquitin chains and be conjugated to substrate proteins,[21] imparting various cellular signals for processes, like proteasomal degradation, inflammation, and cell cycle regulation.[22−24] Notably, Ub exhibits high thermal stability, yet a fraction is unfolded and degraded alongside substrates by the proteasome.[25,26]

In its native folded state, Ub displays significant dynamics that are essential for its function. While previous studies have primarily utilized NMR and IR spectroscopy to probe Ub's conformational dynamics up to the millisecond time scale,[10,19,27−32] research on slower (ms−s) dynamics has recently emerged, spurred by investigations of phosphorylated ubiquitin (pUb).[33,34] Phosphorylation at S65 by PINK1 kinase "induces" an alternative "retracted-state" conformation for ∼50% of pUb molecules, distinct from the native fold of

Received: July 19, 2024
Revised: August 7, 2024
Accepted: August 7, 2024
Published: August 14, 2024

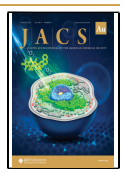

"relaxed-state" due to a shifted C-terminal β-strand (β5) register.[33,35] However, this retracted state is minimally populated for the unmodified wildtype Ub, which only becomes observable at elevated temperatures.[34]

Here, we show that introducing alanine point mutations in Ub β5 modulates the relative population and millisecond-time scale interconversion between relaxed and retracted states. Importantly, our study reveals how suppressing conformational dynamics enhances thermal stability, highlighting the importance of protein dynamics beyond thermodynamic coupling in a static structure.

RESULTS AND DISCUSSION

Alanine Mutations in β5 Differentially Modulate Ub Thermal Stability

We introduced single alanine mutations to residues L67, L69, L71, and L73, all located within the inward-facing β5 strand of Ub. In the relaxed state, L67 and L69 side chains are buried in the hydrophobic core, L71 is partially buried, and L73 resides within the solvent-exposed flexible C-terminal tail. Shown by previous structural studies of pUb,[33,35,36] L69 and L71 are fully buried in the retracted state, while L67 and L73 are partially buried due to altered hydrogen bonding patterns involving β5 (Figure 1).

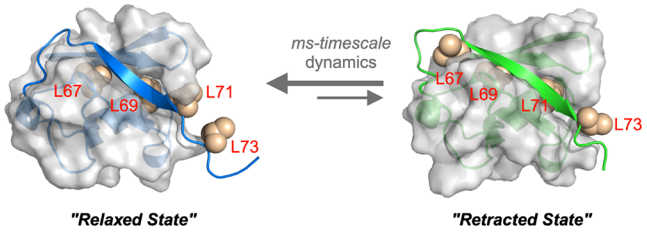

Figure 1. Ub dynamically interconverts at millisecond time scale between two conformational states, i.e., the relaxed state and retracted state. In the latter, β5 moves up or retracts by two residues, thus burying a different set of hydrophobic residues and resulting in an alternative hydrogen-bond pattern. For Ub wildtype, the population of the retracted state is extremely low at ambient temperature ($\ll$1%).

We assessed the thermal stability of Ub wild-type and mutant proteins using differential scanning fluorometry (DSF), leveraging the intrinsic tyrosine fluorescence. Temperature-dependent changes in the ratio of fluorescence intensities at 350 and 330 nm enabled us to determine the melting temperatures (T_m) (Figures 2A and S1A).[37] The L67A and L69A mutants exhibit lower T_m values compared to wildtype Ub. In contrast, the L71A and L73A mutations increased T_m, with the L73A mutant approaching 100 °C (Figure 2A and Table S1).

We further investigated the thermal stability of the various Ub proteins by using Fourier-transformed infrared (FTIR) spectroscopy at increasing temperatures. Overall, wildtype Ub, L67A, and L69A mutants exhibit significant changes in FTIR spectra at elevated temperatures, while L71A and L73A mutants show minimal changes (Figure S1). Second derivative analysis of the FTIR spectra enhanced the resolution of overlapping peaks and revealed subtle changes in the peak positions (Figure 2). Upon heating, the dip at 1641 cm^{-1}, characteristic of intramolecular β-sheet structure, shifts to 1632 cm^{-1} for all Ub constructs, suggesting enhanced structural dynamics in protein folded state.[38] Notably, the L67A mutant exhibited a 1632 cm^{-1} dip in a narrow temperature range, which was immediately replaced by an increasing 1619 cm^{-1} dip, characteristic of intermolecular β-strand formation and protein aggregation.[19,38,39] This was corroborated by the visible clouding and precipitate formation in all FTIR cells except for the L73A mutant (Figure S2).

Importantly, the sharp descent of the 1632 cm^{-1} dip and concurrent rise of the 1619 cm^{-1} dip correlate with the T_m values obtained from the DSF measurements. While this transition occurs only at the highest temperature (99 °C) for the L71A mutant, the 1632 cm^{-1} dip progressively decreases for the L73A mutant without any reversal. Conversely, the L69A mutant shows the 1632 cm^{-1} dip alongside the 1641 cm^{-1} dip even at ambient temperature, corresponding to a broader amide-I band in the raw FTIR data (Figure S1).

To further assess temperature-dependent secondary structure changes, we employed circular dichroism (CD) spectroscopy. With increasing temperature, the CD values between 200 and 210 nm for the L69A mutant are more negative than those for the wildtype or L67A mutant (Figure S3), indicating a greater loss of β-sheet structure in this mutant while retaining most secondary structures.

L67A Mutation Promotes the Retracted State

To investigate the underlying mechanism for the altered thermal stability of the Ub mutants, we turned to NMR spectroscopy. The $^{1}H-^{15}N$ heteronuclear single-quantum coherence (HSQC) spectrum for the L73A mutant closely matched that of the wildtype Ub, except for the residues near the mutation site (Figure S4). On the other hand, the L71A and L69A mutations caused minor perturbations to the HSQC spectra, and affected nearby residues in β2 and β3 (Figures S5 and S6). Notably, the HSQC spectrum of L67A mutant displays more peaks than the total number of nonproline residues in Ub (Figure 3A), indicating the presence of multiple conformational states. Indeed, two sets of peaks with different intensities could be picked and assigned.

The distinct peaks of the Ub L67A mutant can be attributed to two slowly interconverting species (Figure 3A). At 298 K, the major and minor species constitute approximately 78% and 22% of the population, respectively. While the major species exhibits extensive chemical shift differences from wild-type Ub, affecting nearly all β-sheet residues (Figure 3B), the minor species shows much smaller deviations from the wild-type species (Figure 3C). This suggests that the major species corresponds to Ub retracted state, consistent with the previous findings, where mutation of L67 to a polar residue induced near-complete conversion.[34] Further supporting this, Cα and Cβ chemical shifts of residues R72 and L73 in the major species exhibit characteristic β-sheet values (Figure S7A). Additionally, the L67A mutant enabled us to assess the thermodynamics of the relaxed-to-retracted conversion, revealing an endothermic enthalpic change (ΔH) of 16.93 kJ/mol, as the retracted state (major species) becomes more populated with increasing temperature (Figure S7B,C).

L69A Mutation Kinetically Facilitates the Transitioning to the Retracted State

We further employed chemical exchange saturation transfer (CEST) NMR[40] on the Ub L67A mutant to assess the total exchange rate k_{ex}, encompassing both forward (k_{nm}) and reverse exchange (k_{mn}) kinetic rates between major (m) and minor (n) states. Measuring at two $B1$ fields at 318 K yielded a k_{ex} value of 29.56 ± 7.00 s^{-1} (k_{nm} = 28.44 ± 7.00 s^{-1}, k_{mn} =

https://doi.org/10.1021/jacsau.4c00649
JACS Au 2024, 4, 3310−3320

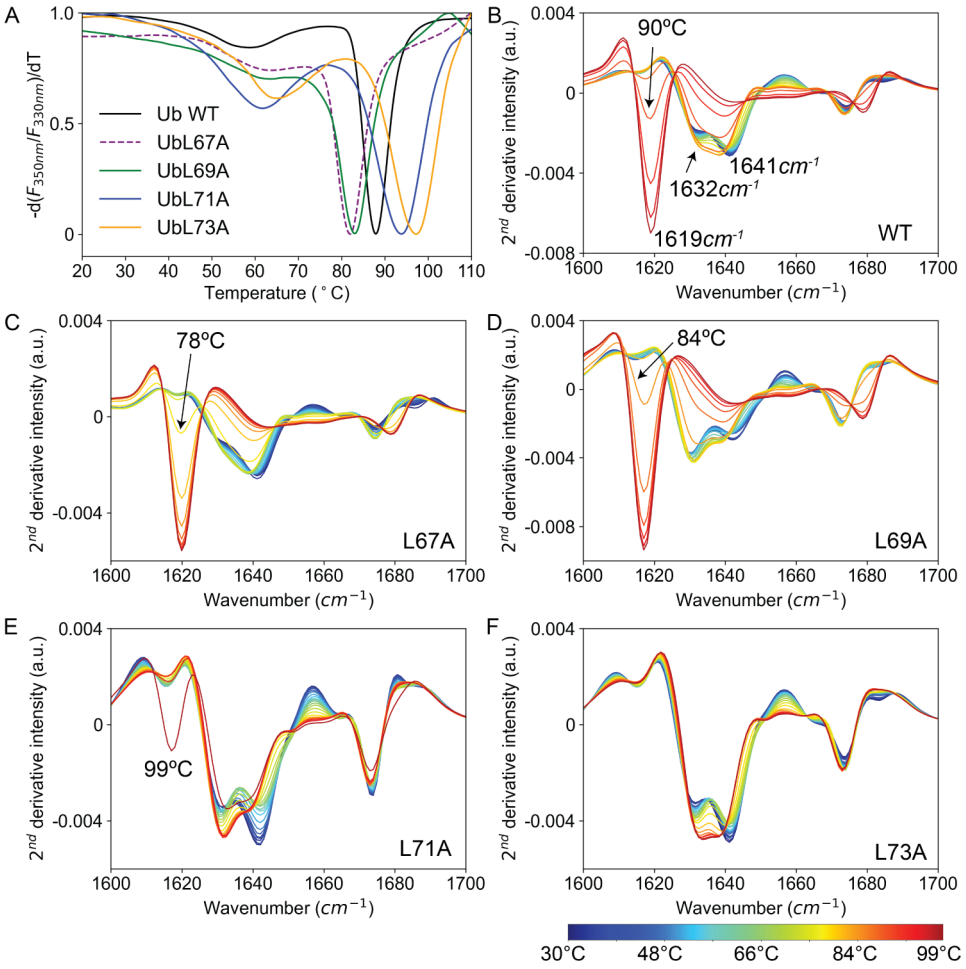

Figure 2. Structural changes of Ub proteins upon thermal denaturation were assessed by DSF and FTIR. (A) First derivatives of 350 nm/330 nm fluorescence intensity ratio for wildtype Ub and L67A, L69A, L71A, and L73A mutants. Three biological replicates were performed using DSF. Determined T_m values (the inflection point in the first derivative curve of 350 nm/330 nm fluorescence intensity ratio) are presented in Table S1. (B–F) Overlaid second derivative FT-IR spectra for the five Ub proteins, as temperature increases from 30 to 99 °C. Labeled vibrational bands are discussed in the text. The transition temperatures for the sharp descent of the 1632 cm^{-1} dip and concurrently sharp rise of the 1619 cm^{-1} dip are also indicated.

1.12 ± 0.04 s^{-1}) (Figure S8, Tables S2 and S3), consistent with the two distinct sets of peaks in L67A HSQC spectrum and comparable to the wildtype Ub k_{ex} of 55.09 ± 14.10 s^{-1} (Figure S9 and Table S4).

For the L69A mutant, we assessed the millisecond dynamics using CEST NMR, and determined the population of the retracted state at 1.30 ± 0.04% at 318 K (Table S5). Notably, the L69A k_{ex} between relaxed and retracted states is 360.23 ± 20.00 s^{-1} (k_{nm} = 355.54 ± 0.04 s^{-1}, k_{mn} = 4.69 ± 0.3 s^{-1}), nearly an order of magnitude faster than the wildtype (Figure 4A). This means that the L69A mutation significantly lowers the energetic barrier between the two Ub conformational states, thereby facilitating the millisecond timescale interconversion.

Additionally, we evaluated the temperature dependence of $^{1}H-^{15}N$ chemical shift values (Figure S10). A temperature coefficient exceeding −4.5 ppb/K indicates reduced hydrogen bonding protection of the amide proton.[41] While wildtype Ub exhibited temperature coefficients consistent with the previous report,[42] the L69A mutant exhibited increased lability. Specifically, residues D32, K33, and I36 at the C-terminus of helix α1 and residues Q41 and R42 at the N-terminus of strand β3 displayed highly negative temperature coefficients (Figures 4B and S11). As these residues cluster near β5, their weakened hydrogen bonding and heightened dynamics suggest transient detachment of β5 during Ub millisecond timescale dynamics.

HDX-MS Reveal Enhanced Structural Dynamics for Ub L67A and L69A Mutants

To further investigate the structural destabilization caused by the point mutations and their correlation with protein dynamics, we used hydrogen–deuterium exchange mass spectrometry (HDX-MS). Comparing the deuterium exchange rates of the peptides derived from wildtype and mutant Ub proteins, we found that the C-terminal peptide of the L69A mutant exchanged more rapidly than that of the L67A mutant (Figures 5 and S12), consistent with its faster millisecond time scale fluctuations. In an EX2 mechanism, the structural element must first undergo opening and partial unfolding, involving hydrogen bond disruption, to allow solvent exchange.[43] Thus, the HDX-MS data support the presence of a transition state characterized by β5 detachment.

Limited exchange data were obtained for the C-terminal residues of wild-type Ub, L71A, and L73A mutants due to proteolysis resistance at the experimental temperature. As expected, L71A and L73A exhibited significantly slower

https://doi.org/10.1021/jacsau.4c00649
JACS Au 2024, 4, 3310–3320

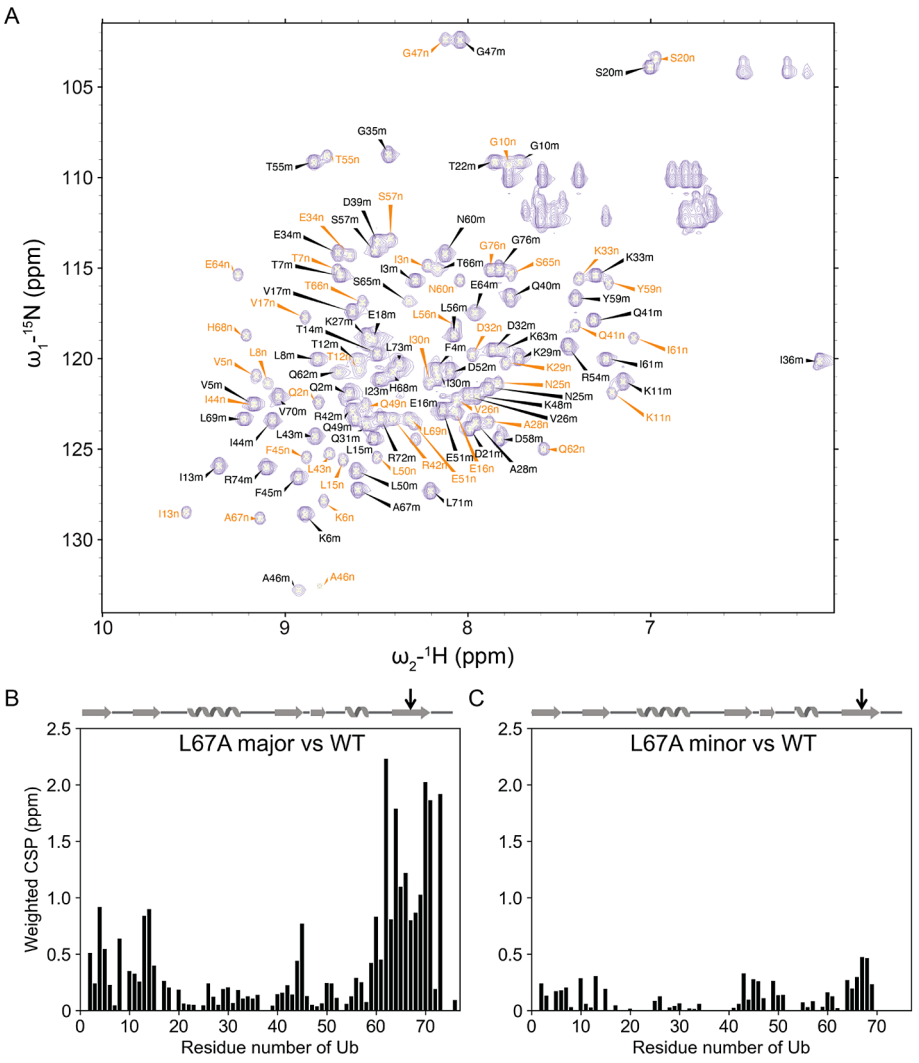

Figure 3. NMR analysis of the Ub L67A mutant. (A) ^{1}H, ^{15}N- HSQC spectrum of the Ub L67A mutant. Peaks in the major (*m*, black labels) and the minor (*n*, orange labels) species of Ub L67A are labeled. (B,C) Chemical shift perturbations (CSPs) between major (B) and minor species (C) of the L67A mutant from Ub wild-type, thus equating the minor species to the relaxed state. Ub secondary structure elements and the mutated residue are denoted at the top of the panels.

exchange rates, particularly at the C- and N-termini, than the wildtype. Elevated temperatures increased exchange (Figure S13), confirming an endothermic process, dependent on overcoming the activation energy for β5 opening. Additionally, N-terminal peptides from L67A and L69A mutants, despite varying charges, displayed faster exchange rates compared to their wild-type counterparts (Figure S14), likely a secondary effect following the detachment of β5.

L71A and L73A Mutations Dampen Ub Millisecond Dynamics

Our CEST measurements for the Ub L71A and L73A mutants revealed an absence of the minor dip in the CEST profiles, suggesting that both mutations negatively impact Ub's millisecond dynamics. Further substantiation for the dampened millisecond dynamics was obtained from phosphorylation rate analysis. PINK1 catalyzes Ub phosphorylation only when the substrate protein adopts the retracted state, in which residue S65 is exposed and snugly fit into the active site of the kinase.[11] Notably, the phosphorylation rates for both L71A and L73A mutants are much slower than those for wild-type Ub or Ub L69A mutant (Figure S15A). Conversely, phosphorylation of L67A Ub was markedly accelerated compared to that of wildtype Ub, with the modification completed within 8 min (Figure S15B).

MD Simulations Reveal Differential Stability of Ub Variants

Molecular dynamics (MD) simulation was employed to assess the structural dynamics of wildtype and mutant Ub proteins in both relaxed and retracted states at 318 K. The simulations revealed no significant differences in the position of β5 relative to the rest of wildtype Ub in either conformational state (Figure S16). Furthermore, the L67A, L71A, and L73A mutations did not substantially alter β5 positions (Figures S17 and S18). However, the L69A mutant exhibited slightly increased fluctuations of the β5 position in both states (Figures S17B and S18B). Additionally, L71A and L73A showed enhanced fluctuations only in the retracted state, though the averaged β5 positions remain largely unchanged (Figure S18C,D).

To further explore the relationship between millisecond dynamics and thermal stability, we conducted MD simulations at an elevated temperature (400 K). Starting from the relaxed-

https://doi.org/10.1021/jacsau.4c00649
JACS Au 2024, 4, 3310−3320

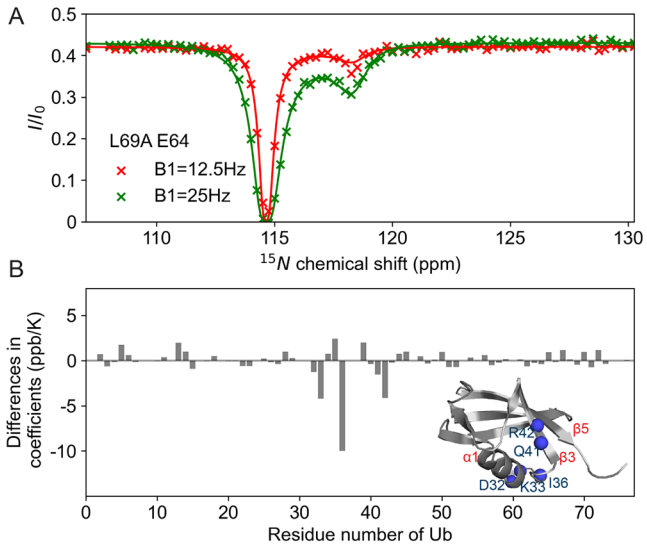

Figure 4. NMR analysis of Ub L69A mutant. (A) L69A mutant undergoes more pronounced millisecond dynamics as assessed with CEST NMR. Representative profile fits for Ub L69A. The exchange rate between major and minor species is determined at ∼360 s^{-1}, with the minor species (retracted state) populated at ∼1.3%. (B) Differences in amide proton temperature coefficients between the Ub L69A mutant and wildtype. Inset, residues with significantly negative temperature coefficients are mapped to the Ub relaxed-state structure.

state structure, wild-type Ub, L71A, and L73A mutants remained folded throughout the simulations, with L73A exhibiting the smallest RMSD fluctuations (Figure 6A). In contrast, Ub L67A mutant began unfolding after 250 ns, characterized with a rapid increase in RMSD, while Ub L69A mutant starts to unfold after 450 ns. The relative order of unfolding aligns with their respective thermal stabilities and dynamics.

Simulations initiated from the retracted state revealed a reversal in stability trends, as L71A and L73A mutants exhibited larger RMSD fluctuations and unfolded earlier compared to wild-type Ub (∼150 ns) (Figure 6B). Conversely, L69A unfolded after 300 ns, consistent with its enhanced dynamics in both relaxed and retracted states. Notably, L67A remained largely folded throughout the simulations, indicating that mutations differentially impact the stability of the two conformational states, with L67A preferentially stabilized in the retracted state.

These extended MD simulations also shed light on the potential transition state ensemble for the millisecond timescale dynamics. Wildtype Ub unfolded only at high temperature when starting from the retracted state. During this unfolding, the C-terminal end of β5 unraveled (Figure 7A), disrupting hydrogen bonds between β5 and β1, consistent with the increased HDX observed for these residues (Figure 5). The L71A and L73A mutations further destabilized the retracted state and accelerated the detachment of β5 from β1 (Figure 7B,C).

DISCUSSION

Our findings demonstrate a fundamental link between Ub's millisecond timescale dynamics and its thermal stability. The presence of a partially unfolded intermediate, characterized by the detachment and disordering of β5, is crucial for both the dynamic interconversion between Ub's relaxed and retracted states and its thermal unfolding process. This suggests that protein stability is not only determined by amino acid interactions within a single folded state but also by the dynamic landscape of conformational fluctuations.

Suppressing millisecond dynamics, specifically the interconversion between relaxed and retracted states, enhances Ub's thermal stability. Conversely, increasing this dynamic behavior reduces the stability. We observed this phenomenon through targeted alanine mutations within strand β5 strand. Mutations near the N-terminus (L67A and L69A) decrease stability, albeit through distinct mechanisms: L67A thermodynamically favors the retracted state, while L69A kinetically enhances the interconversion rate by elevating the energy of both states (Figure 8). In contrast, mutations near the C-terminus (L71A, L73A) dampen millisecond dynamics, leading to increased thermal stability (Figure 8), with the L73A mutant remaining folded even at nearly 100 °C (Figure 2). This demonstrates the potential for significant stability enhancement through a single amino acid substitution.

The β5-detached state observed during partial thermal unfolding likely resembles the Ub folding intermediate, as prior studies have shown that the C-terminal region, including β5, is incorporated into the folded structure at a late stage,[44,45] acting as a "speed-bump" in the folding process at an ambient temperature. This phenomenon of incomplete unfolding, where proteins retain substantial secondary structure while forming intermolecular β-sheets, leading to aggregation and precipitation,[37,38,46] likely extends beyond Ub. Our observation that L69A and L67A mutants exhibit enhanced intermolecular interactions at elevated temperatures (Figure 2) suggests a mechanistic link between the propensity for β5 detachment and aggregation.

Besides implications for protein folding and stability, the dynamic interconversion with the Ub retracted state is physiologically relevant. First, it is a prerequisite for PINK1-mediated phosphorylation, as this kinase specifically accommodates the retracted state.[34] Although wildtype Ub predominantly exists in the relaxed state, the small population of the retracted state is sufficient for phosphorylation and can be resupplied through equilibrium shift. Second, the interconversion likely facilitates Ub degradation. While most Ub is recycled, a small fraction undergoes proteasomal degradation alongside with the substrate.[47,48] The presence of a partially unfolded state would make Ub more susceptible to unfolding and timely degradation. This notion is supported by previous findings showing that replacing L73 with Ala or other polar residues reduces the fitness of yeast strains in harsh environments.[49,50]

In conclusion, our work reveals a vital link between protein millisecond dynamics and stability, underscoring the importance of considering conformational flexibility beyond static structures. This new understanding of protein behavior also has significant implications for protein engineering, design, and our comprehension of cellular proteostasis.

EXPERIMENTAL SECTIONS

Sample Preparation

Wildtype human ubiquitin (Ub) in the pET11a expression vector was subjected to modification using the KOD-Plus-Mutagenesis Kit (TOYOBO, Tokyo, Japan) to introduce mutations L67A, L69A, L71A, or L73A. The Ub, Ub mutants, and *Pediculus humanus corporis* phPINK1 (residues 115 to 575) were expressed and purified as

https://doi.org/10.1021/jacsau.4c00649
JACS Au 2024, 4, 3310−3320

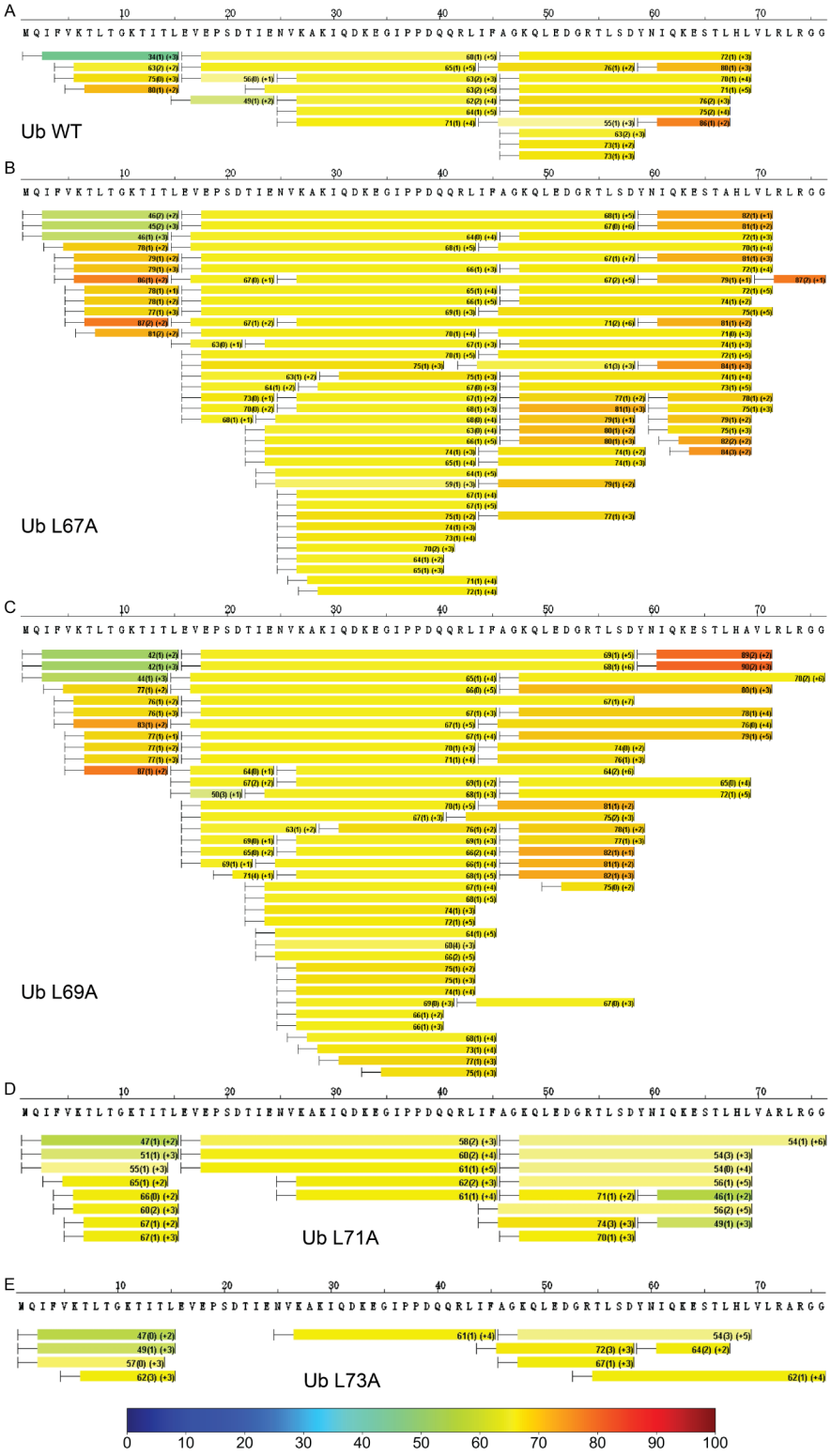

Figure 5. Impact of β5 alanine mutations on Ub protein opening and solvent exchange. Heat maps depict HDX-MS analysis of wild-type (A), L67A (B), L69A (C), L71A (D), and L73A (E) Ub proteins at 323 K following 45 s of D_2O exchange. The color scale at the bottom indicates the percentage of deuterium substitution for labile protons in trypsin-derived peptides.

previously outlined in references.[33,51] For the present study, the phPINK1 protein underwent an additional purification step involving size exclusion chromatography using a Superdex 75 10/300GL column (Cytiva). The column was pre-equilibrated with NMR buffer containing 20 mM HEPES at pH 7.4 and 100 mM NaCl, following the cleavage of the GST-tag facilitated by TEV protease.

Determination of the Thermal Stability of Ub Mutants

The assessment employed two distinct techniques. (1) Intrinsic differential scanning fluorometry (DSF). We utilized a Prometheus NT.48 instrument (NanoTemper Technologies GmbH, Munich, Germany) to determine the melting temperature (T_m) of Ub. This experiment involved measuring intrinsic fluorescence intensity at 330

https://doi.org/10.1021/jacsau.4c00649
JACS Au 2024, 4, 3310−3320

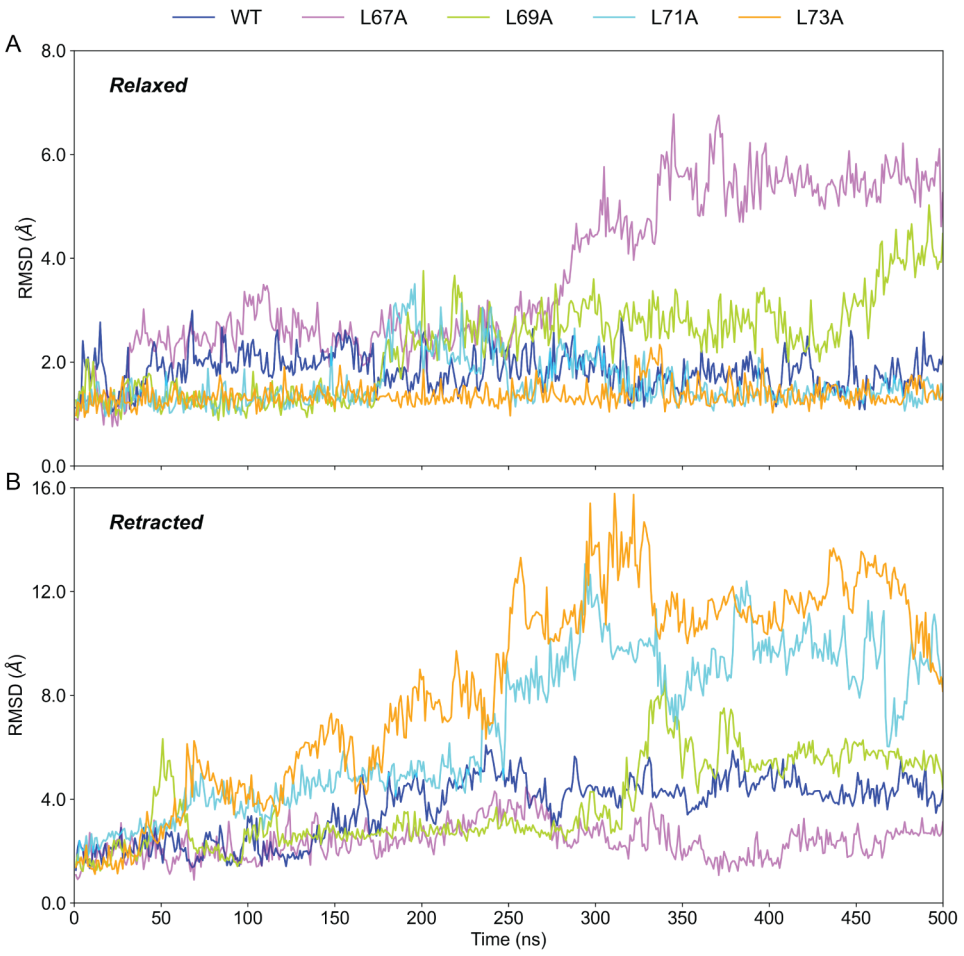

Figure 6. Trajectories of MD simulations at 400 K for the various Ub constructs starting from either the relaxed state (A) or the retracted state (B). Snapshots were taken for every 1 ns and were superimposed to the first frame by backbone heavy atoms.

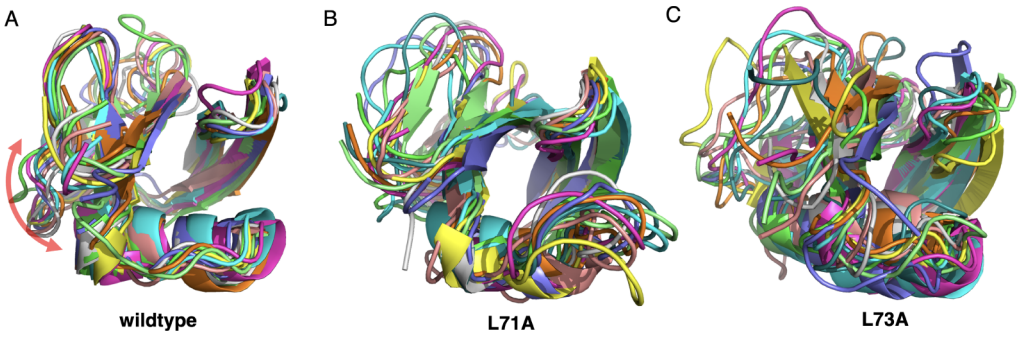

Figure 7. Ub structural changes during high-temperature MD simulations. (A) Superposition of the conformations of wild-type Ub within 200−300 ns simulation window. The red arrow indicates flayed motion of the C-terminus. (B, C) Superposition of the conformations of Ub L71A mutant and Ub L73A mutant, respectively, within 100−200 ns simulation window. The simulations started from the retracted-state structure, and the snapshots were taken every 10 ns.

and 350 nm with excitation at 280 nm. Three consecutive temperature scans were conducted on the same sample (3 × 10 μL) in a linear ramp of 1 °C/min, spanning from 20 to 110 °C. The sample was allowed to equilibrate for 1 min at each temperature point before measurement. The Ub samples were loaded into standard DSF grade capillaries, and all samples were prepared in the same buffer used for NMR. A negative control containing only the NMR buffer was included in each run. The apparent Ub melting temperature (T_m) was determined as the lowest point in the temperature-dependent variation (first derivative) of the 350 nm/330 nm fluorescence ratio, using the ThermControl software V2.1 (NanoTemper Technologies).

(2) Fourier-transformed infrared spectroscopy (FTIR). FTIR absorption spectra were collected by using a Vertex 70 V instrument (Bruker Optics, Germany). Ub protein samples (wildtype or mutants), at a concentration of 10 mg/mL, were placed in a two-compartment CaF_2 sample cell with a 50 μm thick Teflon spacer. Simultaneous measurement of a D_2O reference was conducted. The measurements took place in a custom-built vacuum chamber, with temperature control maintained at an accuracy of ±0.1 °C through water circulation.[52,53] Prior to each measurement, the samples were thermally equilibrated for 4 min, starting from room temperature and extending beyond 100 °C. It is noteworthy that the chamber holding

https://doi.org/10.1021/jacsau.4c00649
JACS Au 2024, 4, 3310−3320

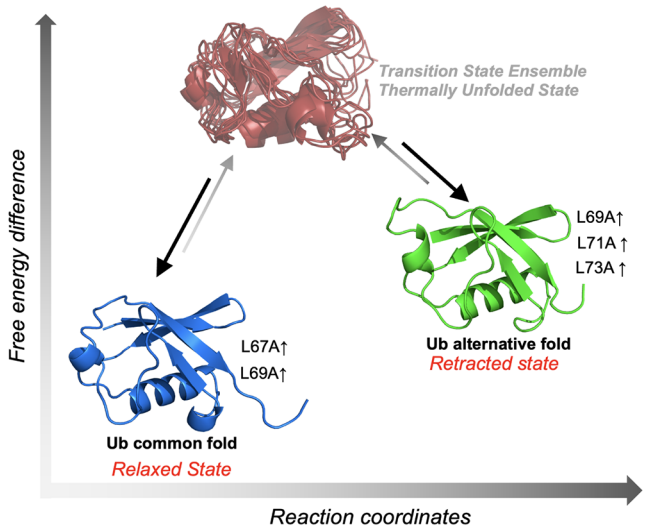

Figure 8. Schematic representation of the relationship between Ub millisecond dynamics and thermal unfolding. Ub dynamically interconverts between the relaxed state (Ub common fold) and the retracted state (Ub alternative fold). The transition state ensemble for this interconversion recapitulates the partially unfolded state formed during thermal denaturation, which may further form intermolecular β-sheets, leading to protein aggregation. The L67A mutation destabilizes the relaxed state, while the L69A mutation destabilizes both the relaxed and retracted states, thereby facilitating their interconversion. Conversely, L71A and L73A mutations strongly destabilize the retracted state, making interconversion less likely.

the L73A mutant remained transparent even after reaching the highest temperature. A second derivative analysis was also performed on the FTIR spectra for further analysis.

NMR Spectroscopy

Nuclear magnetic resonance (NMR) data was acquired at 298 K using a Bruker Avance III HD 800 MHz spectrometer equipped with a cryogenic triple-resonance TCI probe, unless otherwise specified. Data processing utilized Topspin (Bruker) and NMRPipe,[54] while data analysis was carried out with Poky.[55] For backbone chemical shift assignments, NMR samples consisted of 0.4 mM Ub mutants in an NMR buffer comprising 20 mM HEPES (pH 7.4), 100 mM NaCl, and 10% D_2O. The assignments were obtained through the application of standard triple-resonance pulse sequences. Specifically, HNCACB and HN(CA)CO spectra were collected, featuring 2048 × 40 × 100 complex points in the ^{1}H, ^{15}N, and ^{13}C dimensions, respectively. HN(CA)CO spectra employed a nonuniform sampling scheme at a rate of 30% complex points in the ^{1}H, ^{15}N, and ^{13}C dimensions. Subsequently, these spectra were reconstructed using iterative shrinkage thresholding (IST) within the NMRPipe package.[56]

Given the minor chemical shift perturbations observed, cross-peak assignments for the L71A and L73A mutants were accomplished by comparing them to the ^{1}H, ^{15}N-HSQC spectrum of the wildtype. Following the backbone assignment, weighted chemical shift perturbation calculations were calculated as $\sqrt{(\Delta^{1}H)^2 + 0.2 \times (\Delta^{15}N)^2}$, in which Δ denotes the difference in the chemical shift values (ppm) between the cross-peaks of different Ub proteins. Data was plotted with in-house scripts.

The NMR samples for the CEST experiments consisted of 0.4 mM Ub protein in the NMR buffer. CEST measurements were performed using ^{15}N-pseudo-3D CEST experiments at 318 K, employing established pulse sequences.[40] Each experiment involved a total exchange time of 400 ms, a relaxation delay of 1 s, and a B_1 saturation field of either 12.5 or 25 Hz, spanning the ^{15}N range of 107 to 134 ppm with a total of 98 points for Ub L67A, Ub L69A, Ub L71A, and Ub L73A, and 115 points for the wildtype Ub. Peak intensities of residues displaying a distinct minor dip at the two different B1 fields were globally fit using the ChemEX (https://github.com/gbouvignies/ChemEx), affording exchange rates and relative populations. The ^{15}N CEST profiles were plotted as I/I_0 against the applied B_1 field, with the I_0 value extracted from the first transient of the acquisition.

Temperature coefficients of amide protons were determined by recording ^{1}H, ^{15}N-HSQC spectra at 4° intervals, ranging from 286 to 318 K for each Ub mutant. In each spectrum, ^{1}H chemical shifts were referenced to the methyl proton signal of DSS, and signals were assigned using Poky.[55] Amide proton chemical shift (CS) temperature coefficients were calculated as the slope obtained from the linear fitting of the CS over temperature. For cross peaks that disappeared at one or more temperatures, the corresponding data points were excluded.

The phosphorylation of Ub proteins was carried out in the NMR buffer supplemented with 10 mM $MgCl_2$, 10 mM ATP, and 5 mM DTT at 298 K. Ub and phPINK1 were present at concentrations of 108 and 0.4 μM, respectively. Real-time monitoring of Ub phosphorylation was conducted using BEST-HSQC experiments,[57,58] which included eight scans, 128 increments, and a relaxation delay of 400 ms, amounting to approximately 8 min for a single measurement.

Hydrogen–Deuterium Exchange Mass Spectrometry (HDX-MS)

Peptides derived from Ub proteins, including the wild-type L67A, L69A, L71A, and L73A mutants, were identified using LC-MS/MS (ThermoFisher Orbitrap Fusion). Raw data were imported into Proteome Discover 2.4 software to identify high-scoring peptides. For subsequent HDX-MS analysis, 4 μL of purified ubiquitin (wildtype, L67A, L69A, L71A, and L73A each at 8 μM concentration) was mixed with 16 μL of D_2O buffer (50 mM HEPES and 50 mM NaCl, pH 7.5) after incubation at various time points (10, 20, 30, 40, 45, 60, 180, and 300 s) at desired temperatures (323 K, 333 K, and 343 K) in a PCR instrument. Deuterium exchange was quenched by adding 20 μL of ice-cold buffer containing 3 M guanidine hydrochloride and 1% trifluoroacetic acid. Each quenched sample was immediately injected into the LEAP Pal 3.0 HDX platform (Trajan Scientific and Medical). After injection, the samples were passed through an immobilized pepsin column. The digested peptides were captured on a C18 PepMap300 trap column (Thermo Fisher Scientific) and separated across a C18 separator column (Thermo Fisher Scientific). More detailed experimental procedures can be found in the reference.[59] The percentage of deuterium content and statistical significance (unpaired t-test) were analyzed and visualized using HDX Workbench software.[60]

Circular Dichroism Measurement

CD spectra were recorded on a JASCO J-815 spectropolarimeter (JASCO Inc., Tokyo, Japan) at a wavelength from 200 to 250 nm with an interval of 0.5 nm. Three individual scans were conducted on the sample in a linear ramp of 10 °C/min, spanning from 25 to 95 °C. In the experiment, the aqueous solution of each protein (wild-type Ub, Ub L67A, or Ub L69A) with a concentration from 0.3 to 0.5 mg/mL in CD buffer containing 20 mM potassium phosphorate and 120 mM potassium chloride (pH 7.4) was measured.

All-Atom MD Simulations at Two Different Temperatures

Long-time (300 to 500 ns) all-atom molecular dynamic simulations were performed on the relaxed-state Ub structure (PDB code 1D3Z)[61] at room temperature (318 K) and an elevated temperature (400 K), respectively. The wild-type Ub and its four mutants (L67A, L69A, L71A, and L73A) were selected for constructing different Ub systems. In addition, we also prepared Ub structures in the retracted state, which was generated by reverting the pSer residue back to a regular serine with the phosphoryl group removed, using PDB structure 5XK4.[35] The ff99SB force field[62] was applied to produce the parameters for the protein, by using the LEaP module in the AMBER 2021 package.[63] Each system was then solvated in an octahedral periodic box of TIP3P water molecules with a minimum distance of 10.0 Å between the outermost protein atoms and the walls of the simulation box.

https://doi.org/10.1021/jacsau.4c00649
JACS Au 2024, 4, 3310−3320

For simulations at 318 K, the water molecules and counterions were minimized with 10,000 steps of steepest descent, followed by 20,000 steps of conjugate gradient. Then the whole system was minimized with 15,000 steps of steepest descent, followed by 35,000 steps of conjugate gradient to remove the bad contacts. Distance fluctuations were assessed using the cpptraj module within AMBER. The system was then gradually heated to 400 K in 500 ps simulation in the NVT ensemble and then equilibrated for another 500 ps simulation, with weak restraints were performed on the Cα atoms to ensure the accomplishment of the stabilization before reaching the desired temperature. Finally, a 300−500 ns MD simulation, with time step set to 2 fs, was carried out with the NPT ensemble. A SHAKE algorithm[64] was applied to constrain all bonds involving hydrogen atoms. Particle mesh−Ewald (PME) method[65] was used to calculate the electrostatic interactions.

■ ASSOCIATED CONTENT

Supporting Information

The Supporting Information is available free of charge at https://pubs.acs.org/doi/10.1021/jacsau.4c00649.

Figures depicting FT-IR and CD spectra of Ub variants at elevated temperatures, NMR analysis of chemical shift perturbations, van't Hoff analysis of conformational interconversion, CEST NMR analysis of wildtype Ub and L67A mutant, temperature coefficients mapped onto Ub structures, HDX-MS data for Ub variants with a focus on N- and C-terminal fragments, and MD simulation assessment of the fluctuation of C-terminal fragment. Tables provide DSF-derived T_m values and CEST-derived populations and exchange rates (PDF)

■ AUTHOR INFORMATION

Corresponding Authors

Jie Zheng − *Shanghai Institute of Virology, Shanghai Jiao Tong University School of Medicine, Shanghai 200025, China;* orcid.org/0000-0001-7932-5753; Email: jiezheng@shsmu.edu.cn

Jin Wang − *Department of Chemistry and Physics, Stony Brook University, Stony Brook, Newyork 11794-3400, United States;* orcid.org/0000-0002-2841-4913; Email: jin.wang.1@stonybrook.edu

Chun Tang − *Beijing National Laboratory for Molecular Sciences, College of Chemistry and Molecular Engineering, Peking University, Beijing 100871, China; Center for Quantitative Biology, PKU-Tsinghua Center for Life Sciences, Academy for Advanced Interdisciplinary Studies, Peking University, Beijing 100871, China;* orcid.org/0000-0001-6477-6500; Email: Tang_Chun@pku.edu.cn

Authors

Xue-Ni Hou − *Beijing National Laboratory for Molecular Sciences, College of Chemistry and Molecular Engineering, Peking University, Beijing 100871, China*

Bin Song − *Shanghai Institute of Virology, Shanghai Jiao Tong University School of Medicine, Shanghai 200025, China*

Chang Zhao − *State Key Laboratory of Magnetic Resonance and Atomic Molecular Physics, Innovation Academy for Precision Measurement Science and Technology, Chinese Academy of Sciences, Hubei, Wuhan 430071, China*

Wen-Ting Chu − *State Key Laboratory of Electroanalytical Chemistry, Changchun Institute of Applied Chemistry, Chinese Academy of Sciences, Changchun 130022, China;* orcid.org/0000-0002-3377-389X

Mei-Xia Ruan − *Beijing National Laboratory for Condensed Matter Physics, CAS Key Laboratory of Soft Matter Physics, Institute of Physics, Chinese Academy of Sciences, Beijing 100190, China*

Xu Dong − *State Key Laboratory of Magnetic Resonance and Atomic Molecular Physics, Innovation Academy for Precision Measurement Science and Technology, Chinese Academy of Sciences, Hubei, Wuhan 430071, China;* orcid.org/0000-0001-5800-7115

Ling-Shen Meng − *Beijing National Laboratory for Molecular Sciences, College of Chemistry and Molecular Engineering, Peking University, Beijing 100871, China*

Zhou Gong − *State Key Laboratory of Magnetic Resonance and Atomic Molecular Physics, Innovation Academy for Precision Measurement Science and Technology, Chinese Academy of Sciences, Hubei, Wuhan 430071, China*

Yu-Xiang Weng − *Beijing National Laboratory for Condensed Matter Physics, CAS Key Laboratory of Soft Matter Physics, Institute of Physics, Chinese Academy of Sciences, Beijing 100190, China*

Complete contact information is available at: https://pubs.acs.org/10.1021/jacsau.4c00649

Author Contributions

○X.-N.H. and B.S.contributed equally. X.-N.H., and C.T. designed the research; X.-N.H., and C.Z. purified protein samples; X.-N.H., B.S., C.Z., W.-T.C., L.-S.M., and M.-X.R. performed experiments and analyzed the data; Y.X.W., X.D., Z.G., J.Z., and J.W. helped with data analysis; and X.-N.H., B.S., and C.T. wrote the manuscript. CRediT: **Xue-Ni Hou** data curation, formal analysis, investigation, methodology, writing-original draft, writing-review & editing; **Bin Song** data curation, formal analysis, methodology, writing-original draft, writing-review & editing; **Chang Zhao** data curation, formal analysis, methodology; **Wen-Ting Chu** data curation, formal analysis, methodology; **Mei-Xia Ruan** data curation, methodology; **Xu Dong** data curation, supervision; **Ling-Shen Meng** data curation, investigation; **Zhou Gong** data curation, supervision; **Yuxiang Weng** data curation, supervision; **Jie Zheng** data curation, formal analysis, supervision, validation, writing-original draft; **Jin Wang** investigation, methodology, supervision, validation, writing-original draft; **Chun Tang** conceptualization, formal analysis, funding acquisition, investigation, methodology, project administration, supervision, writing-original draft, writing-review & editing.

Notes

The authors declare no competing financial interest.

■ ACKNOWLEDGMENTS

This work has been supported by the funds from the National Key R&D Program of China (2023YFF1204400 to C.T.) and the National Natural Science Foundation of China (92353304 and 22161132013 to C.T.). NMR experiments have been conducted at the Beijing NMR Center and the NMR facility of the National Center for Protein Sciences at Peking University, and the BioNMR facility, Tsinghua University Branch of China National Center for Protein Sciences (Beijing). We thank Dr. Ning Xu (Tsinghua University) for assistance with NMR data collection.

REFERENCES

(1) Anishchenko, I.; Pellock, S. J.; Chidyausiku, T. M.; Ramelot, T. A.; Ovchinnikov, S.; Hao, J.; Bafna, K.; Norn, C.; Kang, A.; Bera, A. K.; DiMaio, F.; Carter, L.; Chow, C. M.; Montelione, G. T.; Baker, D. De Novo Protein Design by Deep Network Hallucination. *Nature* **2021**, *600* (7889), 547−552.

(2) Abramson, J.; Adler, J.; Dunger, J.; Evans, R.; Green, T.; Pritzel, A.; Ronneberger, O.; Willmore, L.; Ballard, A. J.; Bambrick, J.; Bodenstein, S. W.; Evans, D. A.; Hung, C.-C.; O'Neill, M.; Reiman, D.; Tunyasuvunakool, K.; Wu, Z.; Žemgulytė, A.; Arvaniti, E.; Beattie, C.; Bertolli, O.; Bridgland, A.; Cherepanov, A.; Congreve, M.; Cowen-Rivers, A. I.; Cowie, A.; Figurnov, M.; Fuchs, F. B.; Gladman, H.; Jain, R.; Khan, Y. A.; Low, C. M. R.; Perlin, K.; Potapenko, A.; Savy, P.; Singh, S.; Stecula, A.; Thillaisundaram, A.; Tong, C.; Yakneen, S.; Zhong, E. D.; Zielinski, M.; Žídek, A.; Bapst, V.; Kohli, P.; Jaderberg, M.; Hassabis, D.; Jumper, J. M. Accurate Structure Prediction of Biomolecular Interactions with AlphaFold 3. *Nature* **2024**, *630* (8016), 493−500.

(3) Ye, S.; Hsiung, C.-H.; Tang, Y.; Zhang, X. Visualizing the Multistep Process of Protein Aggregation in Live Cells. *Acc. Chem. Res.* **2022**, *55* (3), 381−390.

(4) Fawzi, N. L.; Chubukov, V.; Clark, L. A.; Brown, S.; Head-Gordon, T. Influence of Denatured and Intermediate States of Folding on Protein Aggregation. *Protein Sci.* **2005**, *14* (4), 993−1003.

(5) Oyen, D.; Fenwick, R. B.; Aoto, P. C.; Stanfield, R. L.; Wilson, I. A.; Dyson, H. J.; Wright, P. E. Defining the Structural Basis for Allosteric Product Release from *E. Coli* Dihydrofolate Reductase Using NMR Relaxation Dispersion. *J. Am. Chem. Soc.* **2017**, *139* (32), 11233−11240.

(6) Boehr, D. D.; McElheny, D.; Dyson, H. J.; Wright, P. E. The Dynamic Energy Landscape of Dihydrofolate Reductase Catalysis. *Science* **2006**, *313* (5793), 1638−1642.

(7) Bhabha, G.; Lee, J.; Ekiert, D. C.; Gam, J.; Wilson, I. A.; Dyson, H. J.; Benkovic, S. J.; Wright, P. E. A Dynamic Knockout Reveals That Conformational Fluctuations Influence the Chemical Step of Enzyme Catalysis. *Science* **2011**, *332* (6026), 234−238.

(8) Torgeson, K. R.; Clarkson, M. W.; Granata, D.; Lindorff-Larsen, K.; Page, R.; Peti, W. Conserved Conformational Dynamics Determine Enzyme Activity. *Sci. Adv.* **2022**, *8* (31), No. eabo5546.

(9) Munro, J. B.; Gorman, J.; Ma, X.; Zhou, Z.; Arthos, J.; Burton, D. R.; Koff, W. C.; Courter, J. R.; Smith, A. B., III; Kwong, P. D.; Blanchard, S. C.; Mothes, W. Conformational Dynamics of Single HIV-1 Envelope Trimers on the Surface of Native Virions. *Science* **2014**, *346* (6210), 759−763.

(10) Lange, O. F.; Lakomek, N.-A.; Farès, C.; Schröder, G. F.; Walter, K. F. A.; Becker, S.; Meiler, J.; Grubmüller, H.; Griesinger, C.; Groot, B. L. D. Recognition Dynamics Up to Microseconds Revealed from an RDC-Derived Ubiquitin Ensemble in Solution. *Science* **2008**, *320* (5882), 1471−1475.

(11) Schubert, A. F.; Gladkova, C.; Pardon, E.; Wagstaff, J. L.; Freund, S. M. V.; Steyaert, J.; Maslen, S. L.; Komander, D. Structure of PINK1 in Complex with Its Substrate Ubiquitin. *Nature* **2017**, *552* (7683), 51−56.

(12) Henzler-Wildman, K. A.; Lei, M.; Thai, V.; Kerns, S. J.; Karplus, M.; Kern, D. A Hierarchy of Timescales in Protein Dynamics Is Linked to Enzyme Catalysis. *Nature* **2007**, *450* (7171), 913−916.

(13) Khorasanizadeh, S.; Peters, I. D.; Roder, H. Evidence for a Three-State Model of Protein Folding from Kinetic Analysis of Ubiquitin Variants with Altered Core Residues. *Nat. Struct. Biol.* **1996**, *3* (2), 193−205.

(14) Rea, A. M.; Simpson, E. R.; Meldrum, J. K.; Williams, H. E. L.; Searle, M. S. Aromatic Residues Engineered into the β-Turn Nucleation Site of Ubiquitin Lead to a Complex Folding Landscape, Non-Native Side-Chain Interactions, and Kinetic Traps. *Biochemistry* **2008**, *47* (48), 12910−12922.

(15) Krantz, B. A.; Sosnick, T. R. Distinguishing between Two-State and Three-State Models for Ubiquitin Folding. *Biochemistry* **2000**, *39* (38), 11696−11701.

(16) Vallée-Bélisle, A.; Michnick, S. W. Visualizing Transient Protein-Folding Intermediates by Tryptophan-Scanning Mutagenesis. *Nat. Struct. Mol. Biol.* **2012**, *19* (7), 731−736.

(17) Went, H. M.; Jackson, S. E. Ubiquitin Folds through a Highly Polarized Transition State. *Protein Eng., Des. Sel.* **2005**, *18* (5), 229−237.

(18) Sabelko, J.; Ervin, J.; Gruebele, M. Observation of Strange Kinetics in Protein Folding. *Proc. Natl. Acad. Sci. U. S. A.* **1999**, *96* (11), 6031−6036.

(19) Chung, H. S.; Khalil, M.; Smith, A. W.; Ganim, Z.; Tokmakoff, A. Conformational Changes during the Nanosecond-to-Millisecond Unfolding of Ubiquitin. *Proc. Natl. Acad. Sci. U. S. A.* **2005**, *102* (3), 612−617.

(20) Chung, H. S.; Shandiz, A.; Sosnick, T. R.; Tokmakoff, A. Probing the Folding Transition State of Ubiquitin Mutants by Temperature-Jump-Induced Downhill Unfolding. *Biochemistry* **2008**, *47* (52), 13870−13877.

(21) Komander, D.; Rape, M. The Ubiquitin Code. *Annu. Rev. Biochem.* **2012**, *81* (1), 203−229.

(22) Pohl, C.; Dikic, I. Cellular Quality Control by the Ubiquitin-Proteasome System and Autophagy. *Science* **2019**, *366* (6467), 818−822.

(23) Cockram, P. E.; Kist, M.; Prakash, S.; Chen, S.-H.; Wertz, I. E.; Vucic, D. Ubiquitination in the Regulation of Inflammatory Cell Death and Cancer. *Cell Death Differ.* **2021**, *28* (2), 591−605.

(24) Senft, D.; Qi, J.; Ronai, Z. A. Ubiquitin Ligases in Oncogenic Transformation and Cancer Therapy. *Nat. Rev. Cancer* **2018**, *18* (2), 69−88.

(25) Smalle, J.; Vierstra, R. D. The Ubiquitin 26S Proteasome Proteolytic Pathway. *Annu. Rev. Plant Biol.* **2004**, *55* (1), 555−590.

(26) Hershko, A.; Ciechanover, A.; Heller, H.; Haas, A. L.; Rose, I. A. Proposed Role of ATP in Protein Breakdown: Conjugation of Protein with Multiple Chains of the Polypeptide of ATP-Dependent Proteolysis. *Proc. Natl. Acad. Sci. U. S. A.* **1980**, *77* (4), 1783−1786.

(27) Tjandra, N.; Feller, S. E.; Pastor, R. W.; Bax, A. Rotational Diffusion Anisotropy of Human Ubiquitin from 15N NMR Relaxation. *J. Am. Chem. Soc.* **1995**, *117* (50), 12562−12566.

(28) Fushman, D.; Cowburn, D. Model-Independent Analysis of 15N Chemical Shift Anisotropy from NMR Relaxation Data. Ubiquitin as a Test Example. *J. Am. Chem. Soc.* **1998**, *120* (28), 7109−7110.

(29) Carlomagno, T.; Maurer, M.; Hennig, M.; Griesinger, C. Ubiquitin Backbone Motion Studied via NHN−C'Cα Dipolar−Dipolar and C'−C'Cα/NHN CSA−Dipolar Cross-Correlated Relaxation. *J. Am. Chem. Soc.* **2000**, *122* (21), 5105−5113.

(30) Massi, F.; Grey, M. J.; Palmer, A. G., III Microsecond Timescale Backbone Conformational Dynamics in Ubiquitin Studied with NMR R1ρ Relaxation Experiments. *Protein Sci.* **2005**, *14* (3), 735−742.

(31) Dittmer, J.; Bodenhausen, G. Evidence for Slow Motion in Proteins by Multiple Refocusing of Heteronuclear Nitrogen/Proton Multiple Quantum Coherences in NMR. *J. Am. Chem. Soc.* **2004**, *126* (5), 1314−1315.

(32) Palmer, A. G.; Massi, F. Characterization of the Dynamics of Biomacromolecules Using Rotating-Frame Spin Relaxation NMR Spectroscopy. *Chem. Rev.* **2006**, *106* (5), 1700−1719.

(33) Wauer, T.; Swatek, K. N.; Wagstaff, J. L.; Gladkova, C.; Pruneda, J. N.; Michel, M. A.; Gersch, M.; Johnson, C. M.; Freund, S. M.; Komander, D. Ubiquitin Ser65 Phosphorylation Affects Ubiquitin Structure, Chain Assembly and Hydrolysis. *Embo J.* **2015**, *34* (3), 307−325.

(34) Gladkova, C.; Schubert, A. F.; Wagstaff, J. L.; Pruneda, J. N.; Freund, S. M.; Komander, D. An Invisible Ubiquitin Conformation Is Required for Efficient Phosphorylation by PINK1. *Embo J.* **2017**, *36* (24), 3555−3572.

(35) Dong, X.; Gong, Z.; Lu, Y.-B.; Liu, K.; Qin, L.-Y.; Ran, M.-L.; Zhang, C.-L.; Liu, Z.; Zhang, W.-P.; Tang, C. Ubiquitin S65 Phosphorylation Engenders a PH-Sensitive Conformational Switch. *Proc. Natl. Acad. Sci. U. S. A.* **2017**, *114* (26), 6770−6775.

https://doi.org/10.1021/jacsau.4c00649
JACS Au 2024, 4, 3310−3320

(36) Kazansky, Y.; Lai, M.-Y.; Singh, R. K.; Fushman, D. Impact of Different Ionization States of Phosphorylated Serine-65 on Ubiquitin Structure and Interactions. *Sci. Rep.* **2018**, *8* (1), 2651.
(37) Kotov, V.; Mlynek, G.; Vesper, O.; Pletzer, M.; Wald, J.; Teixeira-Duarte, C. M.; Celia, H.; Garcia-Alai, M.; Nussberger, S.; Buchanan, S. K.; Morais-Cabral, J. H.; Loew, C.; Djinovic-Carugo, K.; Marlovits, T. C. In-depth Interrogation of Protein Thermal Unfolding Data with MoltenProt. *Protein Sci.* **2021**, *30* (1), 201−217.
(38) Herberhold, H.; Winter, R. Temperature- and Pressure-Induced Unfolding and Refolding of Ubiquitin: A Static and Kinetic Fourier Transform Infrared Spectroscopy Study. *Biochemistry* **2002**, *41* (7), 2396−2401.
(39) Ganim, Z.; Chung, H. S.; Smith, A. W.; DeFlores, L. P.; Jones, K. C.; Tokmakoff, A. Amide I Two-Dimensional Infrared Spectroscopy of Proteins. *Acc. Chem. Res.* **2008**, *41* (3), 432−441.
(40) Vallurupalli, P.; Bouvignies, G.; Kay, L. E. Studying "Invisible" Excited Protein States in Slow Exchange with a Major State Conformation. *J. Am. Chem. Soc.* **2012**, *134* (19), 8148−8161.
(41) Baxter, N. J.; Williamson, M. P. Temperature Dependence of 1H Chemical Shifts in Proteins. *J. Biomol. NMR* **1997**, *9* (4), 359−369.
(42) Morimoto, D.; Walinda, E.; Takashima, S.; Nishizawa, M.; Iwai, K.; Shirakawa, M.; Sugase, K. Structural Dynamic Heterogeneity of Polyubiquitin Subunits Affects Phosphorylation Susceptibility. *Biochemistry* **2021**, *60* (8), 573−583.
(43) Englander, S. W. Protein Foldind Intermediates and Pathways Studied by Hydrogen Exchange. *Annu. Rev. Biophys. Biomol. Struct.* **2000**, *29* (1), 213−238.
(44) Briggs, M. S.; Roder, H. Early Hydrogen-Bonding Events in the Folding Reaction of Ubiquitin. *Proc. Natl. Acad. Sci. U. S. A.* **1992**, *89* (6), 2017−2021.
(45) Alderson, T. R.; Charlier, C.; Torchia, D. A.; Anfinrud, P.; Bax, A. Monitoring Hydrogen Exchange During Protein Folding by Fast Pressure Jump NMR Spectroscopy. *J. Am. Chem. Soc.* **2017**, *139* (32), 11036−11039.
(46) Morimoto, D.; Walinda, E.; Fukada, H.; Sou, Y.-S.; Kageyama, S.; Hoshino, M.; Fujii, T.; Tsuchiya, H.; Saeki, Y.; Arita, K.; Ariyoshi, M.; Tochio, H.; Iwai, K.; Namba, K.; Komatsu, M.; Tanaka, K.; Shirakawa, M. The Unexpected Role of Polyubiquitin Chains in the Formation of Fibrillar Aggregates. *Nat. Commun.* **2015**, *6* (1), 6116.
(47) Shabek, N.; Herman-Bachinsky, Y.; Ciechanover, A. Ubiquitin Degradation with Its Substrate, or as a Monomer in a Ubiquitination-Independent Mode, Provides Clues to Proteasome Regulation. *Proc. Natl. Acad. Sci. U. S. A.* **2009**, *106* (29), 11907−11912.
(48) Sun, H.; Mali, S. M.; Singh, S. K.; Meledin, R.; Brik, A.; Kwon, Y. T.; Kravtsova-Ivantsiv, Y.; Bercovich, B.; Ciechanover, A. Diverse Fate of Ubiquitin Chain Moieties: The Proximal Is Degraded with the Target, and the Distal Protects the Proximal from Removal and Recycles. *Proc. Natl. Acad. Sci. U. S. A.* **2019**, *116* (16), 7805−7812.
(49) Roscoe, B. P.; Thayer, K. M.; Zeldovich, K. B.; Fushman, D.; Bolon, D. N. A. Analyses of the Effects of All Ubiquitin Point Mutants on Yeast Growth Rate. *J. Mol. Biol.* **2013**, *425* (8), 1363−1377.
(50) Mavor, D.; Barlow, K.; Thompson, S.; Barad, B. A.; Bonny, A. R.; Cario, C. L.; Gaskins, G.; Liu, Z.; Deming, L.; Axen, S. D.; Caceres, E.; Chen, W.; Cuesta, A.; Gate, R. E.; Green, E. M.; Hulce, K. R.; Ji, W.; Kenner, L. R.; Mensa, B.; Morinishi, L. S.; Moss, S. M.; Mravic, M.; Muir, R. K.; Niekamp, S.; Nnadi, C. I.; Palovcak, E.; Poss, E. M.; Ross, T. D.; Salcedo, E. C.; See, S. K.; Subramaniam, M.; Wong, A. W.; Li, J.; Thorn, K. S.; Conchúir, S. Ó.; Roscoe, B. P.; Chow, E. D.; DeRisi, J. L.; Kortemme, T.; Bolon, D. N.; Fraser, J. S. Determination of Ubiquitin Fitness Landscapes under Different Chemical Stresses in a Classroom Setting. *eLife* **2016**, *5*, No. e15802.
(51) Hou, X.; Sekiyama, N.; Ohtani, Y.; Yang, F.; Miyanoiri, Y.; Akagi, K.; Su, X.; Tochio, H. Conformational Space Sampled by Domain Reorientation of Linear Diubiquitin Reflected in Its Binding Mode for Target Proteins. *ChemPhyschem* **2021**, *22* (14), 1505−1517.
(52) Li, S.; Wang, R.; Li, D.; Ma, J.; Li, H.; He, X.; Chang, Z.; Weng, Y. Thermal-Triggerd Proteinquake Leads to Disassembly of DegP Hexamer as an Imperative Activation Step. *Sci. Rep.* **2014**, *4* (1), 4834.
(53) Li, H.; Ke, H.; Ren, G.; Qiu, X.; Weng, Y.-X.; Wang, C.-C. Thermal-Induced Dissociation and Unfolding of Homodimeric DsbC Revealed by Temperature-Jump Time-Resolved Infrared Spectra. *Biophys. J.* **2009**, *97* (10), 2811−2819.
(54) Delaglio, F.; Grzesiek, S.; Vuister, G. W.; Zhu, G.; Pfeifer, J.; Bax, A. NMRPipe: A Multidimensional Spectral Processing System Based on UNIX Pipes. *J. Biomol. NMR* **1995**, *6* (3), 277−293.
(55) Lee, W.; Rahimi, M.; Lee, Y.; Chiu, A.; Gorodkin, J. POKY: A Software Suite for Multidimensional NMR and 3D Structure Calculation of Biomolecules. *Bioinformatics* **2021**, *37* (18), 3041−3042.
(56) Stern, A. S.; Donoho, D. L.; Hoch, J. C. NMR Data Processing Using Iterative Thresholding and Minimum l 1-Norm Reconstruction. *J. Magn. Reson.* **2007**, *188* (2), 295−300.
(57) Schanda, P.; Melckebeke, H. V.; Brutscher, B. Speeding Up Three-Dimensional Protein NMR Experiments to a Few Minutes. *J. Am. Chem. Soc.* **2006**, *128* (28), 9042−9043.
(58) Lescop, E.; Schanda, P.; Brutscher, B. A Set of BEST Triple-Resonance Experiments for Time-Optimized Protein Resonance Assignment. *J. Magn. Reson.* **2007**, *187* (1), 163−169.
(59) Song, B.; Chen, Y.; Liu, X.; Yuan, F.; Tan, E. Y. J.; Lei, Y.; Song, N.; Han, Y.; Pascal, B. D.; Griffin, P. R.; Luo, C.; Wu, B.; Luo, D.; Zheng, J. Ordered Assembly of the Cytosolic RNA-Sensing MDA5-MAVS Signaling Complex via Binding to Unanchored K63-Linked Poly-Ubiquitin Chains. *Immunity* **2021**, *54* (10), 2218−2230.E5.
(60) Pascal, B. D.; Willis, S.; Lauer, J. L.; Landgraf, R. R.; West, G. M.; Marciano, D.; Novick, S.; Goswami, D.; Chalmers, M. J.; Griffin, P. R. HDX Workbench: Software for the Analysis of H/D Exchange MS Data. *J. Am. Soc. Mass Spectrom.* **2012**, *23* (9), 1512−1521.
(61) Cornilescu, G.; Marquardt, J. L.; Ottiger, M.; Bax, A. Validation of Protein Structure from Anisotropic Carbonyl Chemical Shifts in a Dilute Liquid Crystalline Phase. *J. Am. Chem. Soc.* **1998**, *120* (27), 6836−6837.
(62) Hornak, V.; Abel, R.; Okur, A.; Strockbine, B.; Roitberg, A.; Simmerling, C. Comparison of Multiple Amber Force Fields and Development of Improved Protein Backbone Parameters. *Proteins: Struct., Funct., Bioinform.* **2006**, *65* (3), 712−725.
(63) Case, D. A.; Aktulga, H. M.; Belfon, K.; Ben-Shalom, I. Y.; Berryman, J. T.; Brozell, S. R.; Cerutti, D. S.; CheathamIII, T. E.; Cisneros, G. A.; Cruzeiro, V. W. D., et al. *Amber 2023*; University of California: San Francisco, 2023.
(64) Kräutler, V.; Gunsteren, W. F. V.; Hünenberger, P. H. A Fast SHAKE Algorithm to Solve Distance Constraint Equations for Small Molecules in Molecular Dynamics Simulations. *J. Comput. Chem.* **2001**, *22* (5), 501−508.
(65) Darden, T.; York, D.; Pedersen, L. Particle Mesh Ewald: An N · log(N) Method for Ewald Sums in Large Systems. *J. Chem. Phys.* **1993**, *98* (12), 10089−10092.

https://doi.org/10.1021/jacsau.4c00649
JACS Au 2024, 4, 3310−3320